Experimental and theoretical study of the temperature and concentration dependence of the short-range order in Pt-V alloys

David Le Bolloc'h and René Caudron
Laboratoire Léon Brillouin, CEA-CNRS CE Saclay 91190 Gif sur Yvette, France
and Laboratoire d'Etude des Microstructures, ONERA-CNRS, Boîte Postale 72, 92322 Châtillon Cedex, France

Alphonse Finel
Laboratoire d'Etude des Microstructures, ONERA-CNRS, Boîte Postale 72, 92322 Châtillon Cedex, France
and Université de Cergy-Pontoise, Groupe de Physique Statistique, 2 Avenue Adolphe Chauvin, 95302 Cergy-Pontoise Cedex, France
(Received 30 July 1997)

We present a detailed theoretical and experimental study of the short-range order in the $Pt_{1-c}V_c$ system at two concentrations ($c=\frac{1}{4}$ and $c=\frac{1}{9}$). *In situ* neutron-scattering experiments were performed in order to measure the short-range-order parameters in the disordered phase. We found a drastic effect of the concentration on the short-range order: in Pt_3V, the diffuse intensity is spread along the $(1k0)$ directions with maxima at the (100) positions, despite the stability at low temperature of a DO_{22} phase. In contrast, the diffuse intensity in Pt_8V displays a splitting around the (100) positions with incommensurate maxima. Through inverse Monte Carlo simulations the two experiments yield, within the Ising model, two sets of effective-pair interactions. Despite quite different short-range-order patterns, the interactions seem nearly concentration independent with a dominant first-neighbors interaction V_1. This concentration independence allows us to predict the ordered states and the ordering temperatures. In particular, at low temperatures, these interactions stabilize a new phase of composition A_5B, which to our knowledge has not been observed until now. Finally, we analyze the origin and behavior of the incommensurate split peaks in Pt_8V within a high-temperature expansion and show analytically that the splitting is due to a large decrease of the influence of V_1 on the short-range order as the concentration and/or the temperature decreases. This analysis shows also that the splitting distance should decrease with increasing temperature, in agreement with our Monte Carlo simulations, and in contrast with all the other alloys which have already been investigated, either experimentally or theoretically. More generally, we discuss the origin of the temperature behavior of a splitting distance in relation with the location in q space of the incommensurate maxima. Using very simple arguments, we show, provided the restriction that the first-neighbor interactions are dominant, that the splitting distance increases or decreases with increasing temperature depending on whether these maxima lie along the $(1k0)$ axis or not. [S0163-1829(98)02502-8]

I. INTRODUCTION

The Pt_3V alloy exhibits a disordered fcc structure at high temperature and an ordered structure on this lattice at low temperature. The ordered ground state has the DO_{22} structure and can be obtained by introducing in each $L1_2$ cube an antiphase boundary (APB) in the (001) planes. Any long period structures (LPS's) can be described by changing the APB density $(1/M)$ per fcc cube. In Pt_3V, such a LPS ($M=4/3$) has been found stable at high temperature in a narrow temperature range close to the order-disorder transition.[1,2] It has also been recently shown that the $L1_2$ structure and a series of LPS's are stabilized when the mean electron concentration is slightly decreased through the addition of a third element.[3,4] Such a situation is typical of a quasidegenerate state, where the energy differences between LPS are very small, or equivalently, where the APB energy is weak.[5,6] This is in agreement with electronic structure calculations which show that the relative stability of DO_{22} and $L1_2$ transition alloys are governed by the value of the number of valence electrons per atom.[7] In this paper, we study the $Pt_{1-c}V_c$ system in its disordered state by neutron diffuse scattering. The ordered DO_{22} structure is built with $\langle 10\frac{1}{2}\rangle$ and $\langle 001\rangle$ waves and the usual mean-field theory predicts that it should occur only when the high-temperature diffuse intensity peaks at $(1\frac{1}{2}0)$ positions, which is the case, for example, in Ni_3V.[8] In contrast, we show here that the diffuse intensity of Pt_3V is spread along the $(1k0)$ direction with maxima at the (100) positions. On the other hand, it is interesting to study the evolution of effective pair interactions (EPI's) as a function of the concentration. According to electronic structure calculations, within the generalized perturbation method,[9] we expect a hierarchy between the EPI and a concentration dependence. Using inverse Monte Carlo (IMC) simulations, two sets of EPI's are deduced from the experiments at $c=\frac{1}{4}$ and $c=\frac{1}{9}$. We show that, despite a strong concentration dependence of the diffuse intensity shape, the EPI are nearly concentration independent, in contradiction with the theory.

II. PRELIMINARIES

A. Microscopic model

Within the generalized perturbation method,[9,10] it has been shown that substitutional binary alloys $A_{1-c}B_c$ may be

described within an Ising model with concentration-dependent EPI. If we affect to each site a spin variable σ_n which takes the value $+1$ or -1 depending on whether site n is occupied by an A or B atom, the ordering energy of a configuration $c_i=(\sigma_1,\sigma_2,\ldots)$ can be written as

$$H=\frac{1}{2}\sum_{nm} V_{nm}\sigma_n\sigma_m+h\sum_n \sigma_n,$$

where h is the chemical potential difference and V_{nm} are the EPI which depend only on the relative vector $\vec{R}_{nm}=\vec{r}_n-\vec{r}_m$ between sites.

The ordering energy H is defined up to a constant term $K(c)$ which, in principle, depends on concentration. This term does not affect the statistical properties at fixed c but it affects the overall shape of the phase diagram, even if the pair interactions were concentration independent. More precisely, the width of a two-phase domain depends on $K(c)$. However, the order-disorder transition temperature at a congruent point is independent of $K(c)$.

In principle, the V_{mn} could be deduced from electronic structure calculations, but the smallest ones amount only to fractions of meV, whereas the calculations deal with binding energies, i.e., some eV: it can be understood why the calculation techniques are not yet sufficiently accurate to compute detailed interactions, and why it has, until now, been better to extract them from local order parameters measured in the disordered state:

$$\alpha(\vec{R}_{nm})=(\langle\sigma_n\sigma_m\rangle-\langle\sigma_n\rangle\langle\sigma_m\rangle)/4c(1-c).$$

Those Warren-Cowley parameters have been determined *in situ* above the order-disorder transition temperature by diffuse neutron scattering. From these experimentally determined static correlations, the first nine EPI's have been deduced using inverse Monte Carlo simulations.

B. Experimental

The bulk stoichiometry of the crystals have been determined using an electron microprobe analysis yielding $c=0.251$ and $c=0.132$ for Pt_3V and Pt_8V, respectively. All the simulations of this paper have taken these concentration shifts into account.

The diffuse scattering of neutrons was performed on the dedicated spectrometer $G44$ at the laboratoire Léon Brillouin, CEA/CNRS Saclay, France. We followed the procedure outlined in Ref. 6: two planes of high symmetry, the (100) and (110) planes were explored with an incident wavelength $\lambda=2.59$ Å and a resolution $\Delta\lambda/\lambda\leqslant 4\times10^{-2}$. The spectrometer is equipped with a vacuum chamber (10^{-6} torr) and a furnace which surrounds the sample and enables us to reach 1670 K. In order to reject the contribution of inelastic scattering, the spectrometer is equipped with a time-of-flight analysis, which allows an energy resolution about 4 meV. In these conditions, we obtain the elastic diffuse scattering for $0.7\leqslant\vec{q}=4\pi\sin\theta/\lambda\leqslant 4.5$ Å^{-1} with 2.5° spacing between detectors and 4° steps in the rotation angle ω of the sample.

The experiments were performed at 1393 K for Pt_3V (113 K above the order-disorder transition), and at 1224 K for Pt_8V (134 K above the transition). From these experimental data, we deduced the elastic-scattering cross section of the sample in Laue units: the intensity measured for the sample was calibrated by a vanadium spectrum made in the same experimental conditions, after subtraction, for both intensities, of the spectra of the empty furnace. The data were corrected of absorption, multiple scattering, and thermal motion (Debye-Waller correction).

C. Data reduction

The general expression for the diffuse intensity scattered by binary alloys at the scattering vector $\vec{q}$ can be written as

$$I(\vec{q})=\sum_{n=1}^{N}\sum_{m=1}^{N} b_n b_m \exp[i\vec{q}\cdot(\vec{r}_n-\vec{r}_m+\vec{u}_n-\vec{u}_m)], \quad (1)$$

where $\vec{r}_n$ is the nth lattice position, b_n is the scattering factor of the atom placed on this site n, and $\vec{u}_n$ is the vector displacement from the lattice position to the true atom position.

Up to now, there is no inverse statistical simulation able to deal with combined effects of chemical order and displacements. However, experimentally, it is possible to single out the local order contribution if the scalar product $\vec{q}\cdot(\vec{u}_n-\vec{u}_m)$ is small compared to unity. Thus, within this hypothesis, the exponential in Eq. (1) can be expanded:[11]

$$\exp[i\vec{q}(\vec{R}_{nm}+\vec{u}_{nm})]=\exp(i\vec{q}\vec{R}_{nm})(1+i\vec{q}\cdot\vec{u}_{nm}+\cdots)$$
$$\text{if } \vec{q}\cdot\vec{u}_{nm}\ll 1.$$

After subtraction of the Bragg intensity and thermodynamic averaging, we can write the total diffuse intensity as a sum of two terms: the short-range order (SRO) contribution $I_{\mathrm{SRO}}(\vec{q})$,

$$I_{\mathrm{SRO}}(\vec{q})=NI_{\mathrm{Laue}}\alpha(\vec{q}),$$

$$\alpha(\vec{q})=\sum_{\vec{R}}\alpha(\vec{R})\exp(i\vec{R}\vec{q}),$$

$$I_{\mathrm{Laue}}=c(1-c)(b_A-b_B)^2,$$

and a mean displacements contribution[12] $I^{(1)}_{\mathrm{dep}}(\vec{q})$, which is stronger far away from the origin:

$$I^{(1)}_{\mathrm{dep}}(\vec{q})=-NI_{\mathrm{Laue}}\sum_{lmn}(h_1\gamma^x_{lmn}+h_2\gamma^y_{lmn}$$
$$+h_3\gamma^z_{lmn})\sin[2\pi(h_1 l+h_2 m+h_3 n)] \quad (2)$$

with

$$\gamma^x_{lmn}=\frac{2\pi}{b_A-b_B}\left\{\left(\frac{1-c}{c}+\alpha_{lmn}\right)\langle X^{AA}_{lmn}\rangle b_A-\left(\frac{c}{1-c}+\alpha_{lmn}\right)\right.$$
$$\left.\times\langle X^{BB}_{lmn}\rangle b_B\right\} \quad (3)$$

$$\vec{u}_{lmn}=X_{lmn}\vec{a}+Y_{lmn}\vec{b}+Z_{lmn}\vec{c},$$

where N is the number of atoms and $(\vec{a},\vec{b},\vec{c})$ are the basic vectors of the fcc cube, (l,m,n) stand for the vector $(\vec{R}_{lmn}$

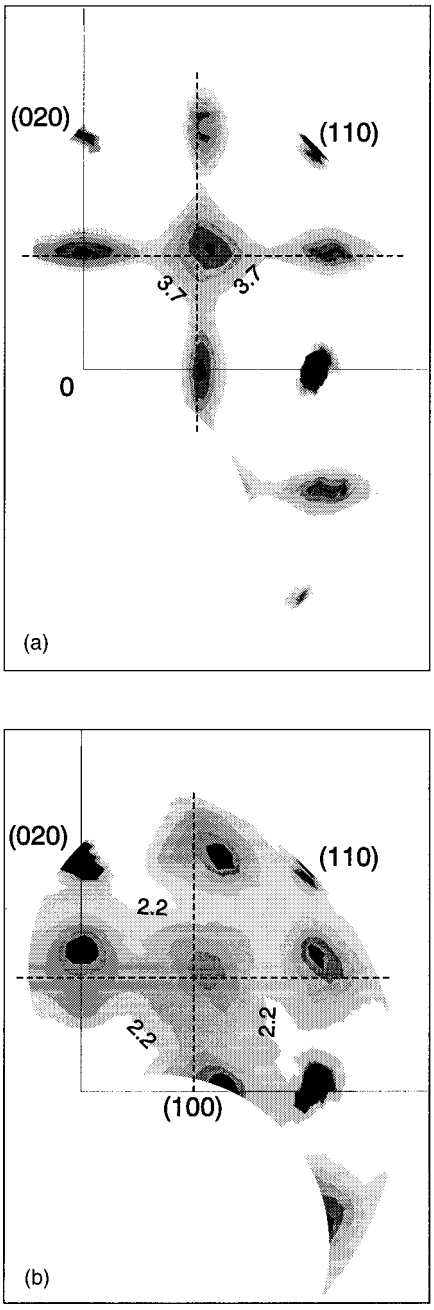

FIG. 1. Experimental total diffuse scattering in the (100) plane in Laue units (a) in Pt_3V and (b) Pt_8V (without absorbtion and multiple scattering). Steps of 0.7 Laue between each contour plots for both maps. Darker regions indicate higher intensity. Larger black areas correspond to the fundamental Bragg peaks. Note that the diffuse intensity maxima in Pt_8V are strongly shifted away from (100).

$=l\vec{a}+m\vec{b}+n\vec{c}$), (h_1,h_2,h_3) designate the coordinates of the scattering vector $\vec{q}=2\pi(h_1\vec{a}^*+h_2\vec{b}^*+h_3\vec{c}^*)$, and $(\vec{a}^*,\vec{b}^*,\vec{c}^*)$ are the unit vectors of the reciprocal space [e.g., $\vec{a}^*=\vec{b}\wedge\vec{c}/\vec{a}\cdot(\vec{b}\wedge\vec{c})$].

From the experimental maps of Fig. 1, the different parameters $[\alpha(\vec{R}_{lmn})=\alpha_{lmn}]$ characterizing the contribution of the local order (the Warren-Cowley parameters) and of the distortions (γ^x_{lmn}) have been fitted using a least-squares method based on a singular value decomposition.

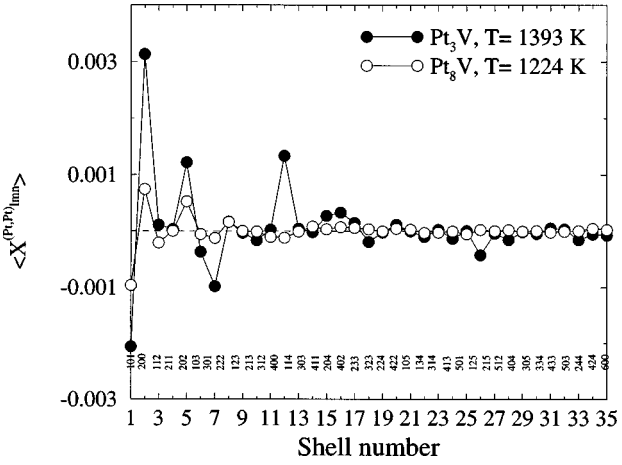

FIG. 2. Experimental values of mean displacements $\langle X^{\mathrm{Pt-Pt}}_{lmn}\rangle$ in lattice units as a function of the shell number in Pt_3V and Pt_8V (the first neighbor in the fcc lattice is noted 101). Their errors bars are smaller than the symbols.

III. EXPERIMENTAL RESULTS

A. Lattice distortions

In our case, the scattering factor of vanadium is negligible compared to that of platinum ($b_V=-0.38$ fm, $b_{Pt}=9.6$ fm). Thus, it is possible from Eq. (3) to compute explicitly the mean values of platinum displacements relative to the perfect fcc lattice ($\langle X^{\mathrm{Pt-Pt}}_{lmn}\rangle$). The mean displacements in Pt_3V and Pt_8V are displayed in Fig. 2. Although the general shape of the modulation is similar for both alloys, the distortions are stronger in Pt_3V. This decrease of the average displacements ($\langle X^{\mathrm{Pt-Pt}}_{lmn}\rangle$) with decreasing concentration is expected since displacements are zero in a pure system.

Yet, the displacements remain sufficiently small in both systems to justify the expansion (2) $[\vec{q}\cdot\vec{u}_{nm}\ll 1;\ \forall(\vec{q},\vec{u}_{nm})]$. As we can see in Fig. 3, the strong shift of the diffuse intensity in Pt_8V is due to a particular shape of the SRO (see below) rather than strong displacements.

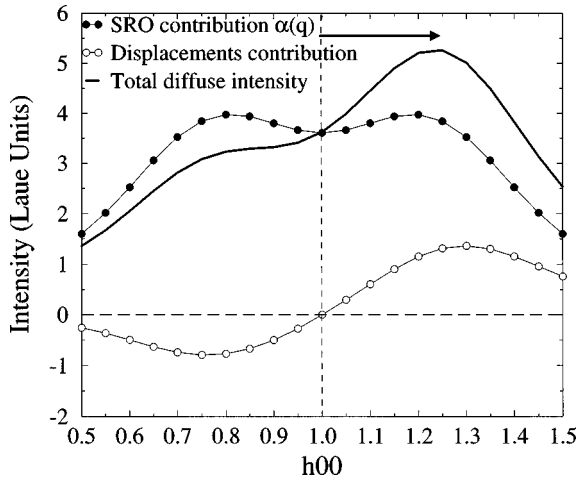

FIG. 3. SRO $\alpha(\vec{q})$, displacements contribution and total diffuse intensity in Pt_8V, along the $(h00)$ direction. Note that the total diffuse intensity maximum is strongly shifted away from the (100) point. Rather than strong displacements effect, this is due to a particular shape of the SRO and a negative contribution of displacements for $h<1$.

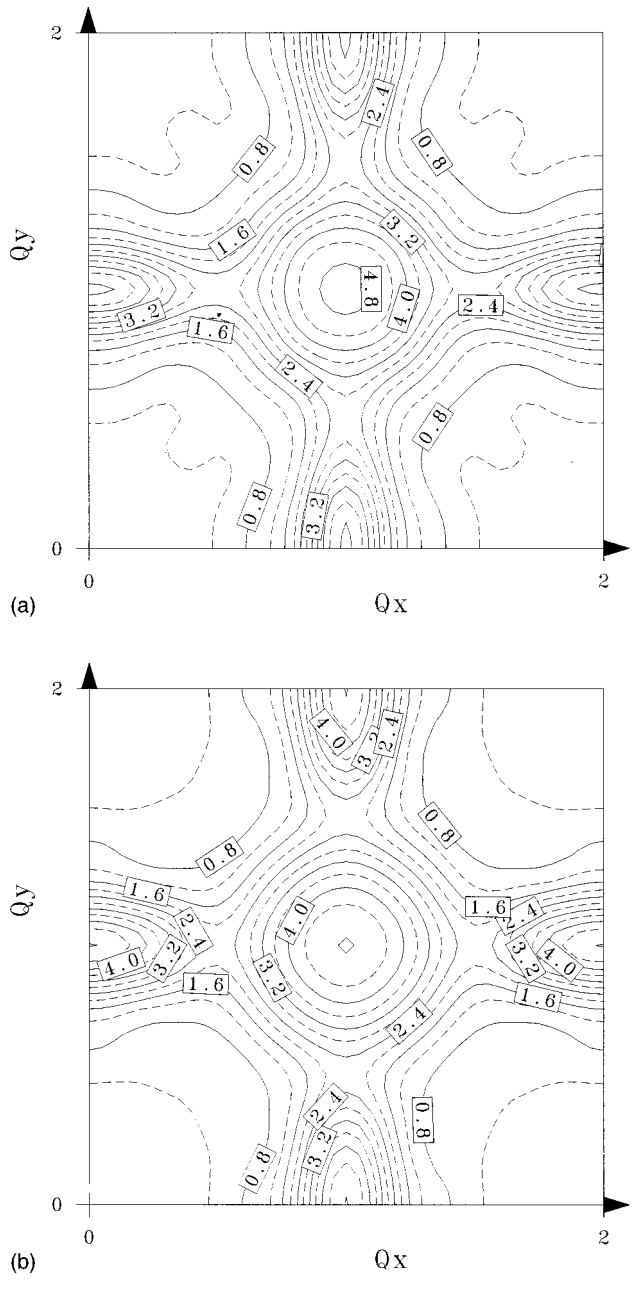

FIG. 4. (a) Experimental SRO contribution in Pt_3V. (b) Simulated SRO with the Pt_3V interaction set (see text).

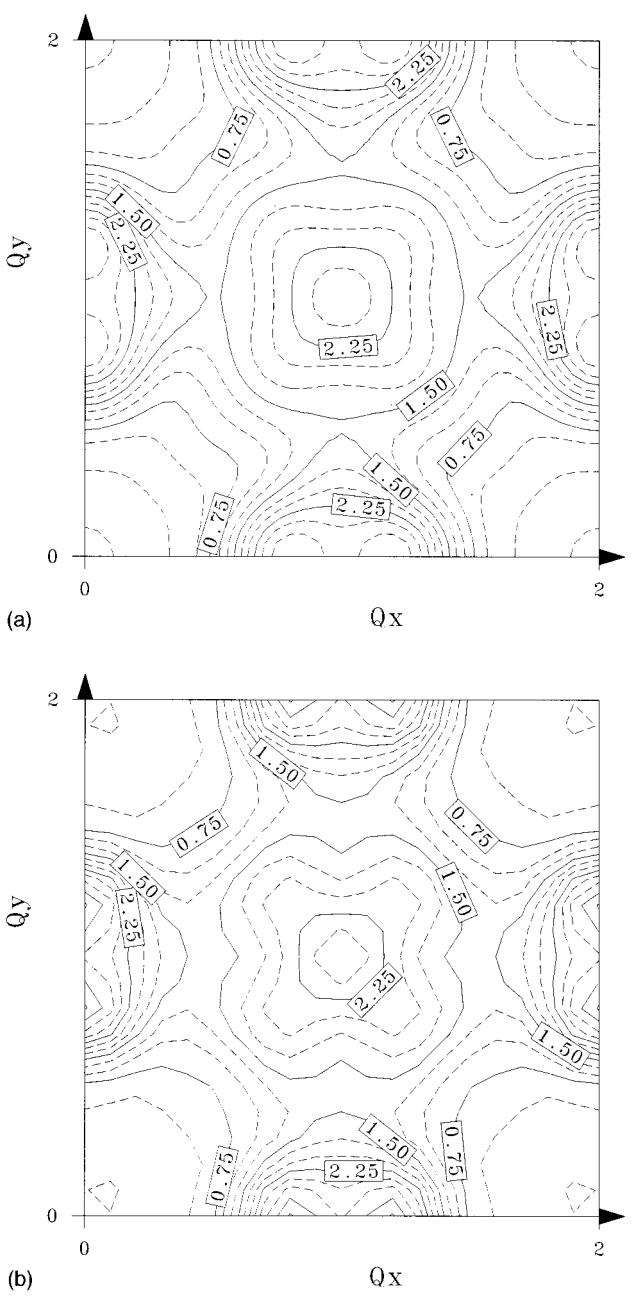

FIG. 5. (a) Experimental SRO contribution in Pt_8V. (b) Simulated SRO with the Pt_8V interaction set (see text).

B. Short-range-order contribution

The SRO intensity distribution $\alpha(\vec{q})$ in the (100) plane are displayed in Figs. 4 and 5 for Pt_3V and Pt_8V, respectively. The corresponding values of $\alpha(\vec{R}_{nm})$ are displayed in Table I.

As for Pd_3V,[5] the diffuse intensity of Pt_3V is spread along the $(1k0)$ direction with maxima at the (100) positions. As discussed in the introduction, these positions of the SRO maxima are not compatible with the DO_{22} ground state within the usual mean-field approach.

We observe a drastic effect of the concentration on the SRO contribution [see Figs. 4(a) and 5(a)]. Indeed, in Pt_8V, the maxima are no longer located at special points of the fcc lattice. Instead, the (100) intensity is split along the (100) axis and presents a saddle point at (100). We note that these maxima are not located just above the superstructures of the ordered state. The Bragg peaks of the A_8B ground state[1] are located at $(\frac{2}{3}00)$ and $(\frac{2}{3}\frac{2}{3}0)$ (and equivalent points), whereas the maximum of the SRO intensity is maximum on an incommensurate position, between $(\frac{2}{3}00)$ and (100).

IV. THEORETICAL INTERPRETATION IN TERMS OF THE ISING MODEL

A. Determination of effective pair interactions

Using an IMC algorithm, we determined a set of nine EPI's for each alloy (we used a simulation box containing 4×18^3 atoms). The results are displayed in Fig. 6 and Table II. For each alloy, the output from the inverse procedure has been used as an input interaction set in a direct MC simula-

TABLE I. Experimental short-range order parameters in Pt_3V and Pt_8V as a function of the shell number.

Shell No.	lmn	$\alpha(Pt_3V)$	$\alpha(Pt_8V)$
1	110	−0.1619(0.0020)	−0.123(0.0012)
2	200	0.2144(0.0022)	0.1505(0.0019)
3	211	−0.00314(0.0016)	−0.0214(0.0009)
4	220	0.0699(0.0015)	0.0215(0.0011)
5	310	−0.0589(0.0010)	−0.0049(0.0008)
6	222	0.0141(0.0013)	0.0121(0.0014)
7	321	−0.0065(0.0006)	−0.002(0.006)
8	400	0.0423(0.0020)	0.0136(0.0016)
9	330	−0.0029(0.0010)	0.0314(0.0010)
10	410	0.0258(0.0010)	−0.0063(0.0007)
11	420	0.0103(0.0012)	−0.0049(0.0007)
12	332	0.00376(0.0060)	0.0072(0.0005)
13	422	−0.0058(0.0007)	−0.0035(0.0005)
14	510	−0.0217(0.0010)	0.0010(0.0005)
15	431	0.0017(0.0005)	−0.0036(0.0004)
16	521	−0.0017(0.0008)	0.0010(0.0003)
17	440	−0.0038(0.0012)	−0.0010(0.0007)
18	530	−0.0021(0.0006)	0.0051(0.0005)
19	433	0.0008(0.0005)	0.0010(0.0004)
20	600	0.0142(0.0019)	0.0014(0.0001)

tion, in order to calculate a diffuse intensity map. In Figs. 4 and 5, we present the two experimental SRO contributions together with the respective Monte Carlo simulations.

The agreement with the experimental maps is very good. All features of the two patterns are well reproduced: the intensity spreads along the (100)-(110) axes with maxima at (100) for Pt_3V, and the characteristic double peak with incommensurate maxima observed in Pt_8V are well reproduced.

B. Comments about the EPI

According to the generalized perturbation method (GPM),[9] a hierarchy between the EPI's is expected, due to the geometry of the fcc lattice. This hierarchy, in terms of first-neighbors steps ($|V_1| \gg |V_2, V_3, V_4| \gg |V_5, V_6, \ldots|$), is well observed, especially with the Pt_8V set. However, despite very different diffuse intensity maps, we find that the interactions are nearly concentration independent (Fig. 6).

This behavior was unexpected, since electronic structure calculations based on the GPM predict that, due to band filling, the V's should vary significantly with concentration. A c-independent behavior of the EPI has already been found in the Ni-Cr system.[13,14,6]

Meanwhile, our result indicates that the long ranged interactions ($V_5, \ldots, V_9$) are significant. In particular, V_9 [which corresponds to the vector $(\frac{3}{2}\frac{3}{2}0)$, in units of the fcc cube] is relatively high and stable for both sets and seems to have a strong influence on the T_c of the A_8B phase (see below). This strong value of V_9 is not a cutoff effect: the V_9 value found within the γ expansion method[15] is consistent with the IMC. Furthermore, this value is stronger than the longer-ranged EPI.

TABLE II. Effective-pair interactions found in Pt_3V and in Pt_8V as a function of the shell number (in meV/atom).

$V(\vec{R})$	V_1	V_2	V_3	V_4	V_5	V_6	V_7	V_8	V_9
$V(Pt_3V)$	44.5	−7	6.3	5.6	4.9	0.19	−0.88	2.3	−4
$V(Pt_8V)$	53.9	−12.8	7.2	9.8	−0.8	−2.3	−0.07	0.5	−4.4

C. Simulated diffuse intensity maps

As explained above, despite the fact that the interactions do not depend on concentration, the diffuse intensity maps of Pt_3V and Pt_8V are very different. This behavior is in contradiction with a mean-field approach: According to the Krivoglaz-Clapp-Moss formula,[16] a minimum of $V(\vec{q})$ corresponds to a maximum of $\alpha(\vec{q})$. So, if the V's do not change with the concentration, the mean-field approach cannot explain the topology changes observed in the diffuse intensity maps.

The above results show that the concentration dependence of the intensity maps is purely a statistical mechanics effect. In order to illustrate this important conclusion, we have computed $\alpha(\vec{q})$ for $c=\frac{1}{9}$ and at a temperature 50 K above the ordering transition of Pt_8V [see Fig. 7(c)], with the V's extracted from the diffuse intensity of Pt_3V. Obviously, this Monte Carlo simulation reproduces the experimentally observed splitting of the diffuse intensity maxima, with a saddle point at (100).

As shown in Fig. 7, the calculated splitting is temperature dependent: with increasing temperature, the incommensurate maxima shift towards the (100) points. A similar result has recently been obtained with the γ expansion method[17,18] using our interaction set.[19] The origin and behavior of these incommensurate diffuse maxima are further discussed below (see Sec. V).

D. Ground states and transition temperatures

We show now that, using the interactions determined above, we nicely reproduce the experimental transition temperatures and properties of the ordered states. This is a strong indication of the temperature transferability of the EPI. A similar agreement has already been obtained for other systems.[6]

1. Ordered state at the Pt_3V composition

The interaction set we obtain at $c=\frac{1}{4}$ stabilizes, at zero temperature, the DO_{23} phase, in contradiction with the experimentally observed DO_{22} phase. However, we stress that the energy difference between DO_{23} and DO_{22} is tiny: within the present approach, this energy difference (per site) amounts to[20]

$$\Delta E(DO_{23}-DO_{22}) = -3.3 \text{ meV}.$$

As for the energy difference between $L1_2$ and $D0_{22}$, we have[20]

$$\Delta E(L1_2-DO_{22}) = -2 \text{ meV}.$$

In fact, these energy differences are essentially zero and, thus, much lower than the result of electronic structure

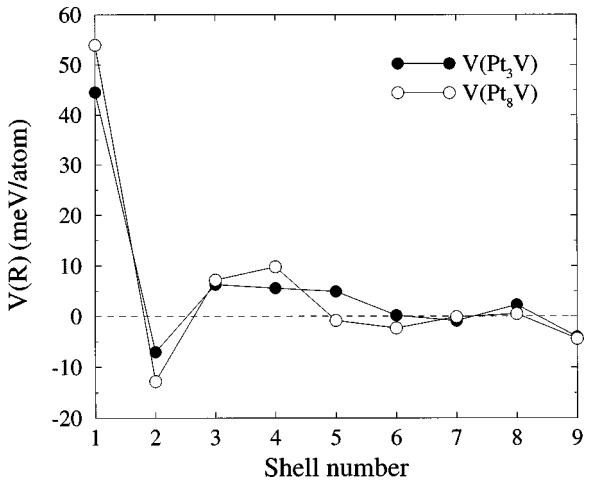

FIG. 6. Pt_3V and Pt_8V interaction set in meV/atom.

calculations that lead to $DE(L1_2-DO_{22})=65$ meV.[21] The same type of discrepancy has already been pointed out for Ni_3V.[22,8]

More generally, we find a very high degeneracy between all LPS's. This is compatible with the experimentally observed degeneracy in Pt_3V: as discussed in the introduction, a small change of the electronic concentration (by adding a few percent of rhodium) leads to a sequence of long period structures that interpolate between $L1_2$ and DO_{22}.[4]

As for the transition temperature between the DO_{23} and disordered states, a MC simulation leads to a $T_c^{\rm cal}\sim 1100$ K, close to the experimental value $T_c^{\rm exp}=1288$ K.

Finally, we mention that the Pt_8V interaction set also leads to a degeneracy at the A_3B composition, with a weak preference for the $L1_2$ phase and a calculated transition temperature close to the experimental one: $T_c^{\rm cal}\sim 1100$ K.

2. Ordered state at the Pt_8V composition

The $c=\frac{1}{9}$ interaction set stabilizes the experimentally observed A_8B phase at zero temperature.[1,2] The fact that we find the correct ground state is a strong indication of the relevance of the long-range part of our interaction set. Indeed, with only four interactions, the ground state at composition $c=\frac{1}{9}$ is degenerated between many A_8B structures.[23] Of course, this degeneracy is expected to be lifted by the interactions beyond V_4. It happens that the numerical values we found for these interactions precisely lift the degeneracy in favor of the experimentally observed A_8B phase. As for the calculated transition temperature, we found $T_c^{\rm cal}\sim 850$ K, which is to be compared to the experimental value $T_c^{\rm exp}=1090$ K.

An analysis at the same composition, but with the Pt_3V interaction set leads to the same A_8B ordered phase, but with a much lower transition temperature: $T_c^{\rm cal}\sim 350$ K. We comment on that point below (see Sec. V).

3. Other ordered states

As the effective interactions seem to vary only weakly with the concentration, we may use them to analyze the phase diagram at concentrations other than $c=\frac{1}{4}$ and $c=\frac{1}{8}$.

First, between the two concentrations where the interactions have been determined, we found a ground state of composition A_5B, noted ''13'' in Kanamori's classification.[23] This ordered state is stabilized with both sets of interactions, with roughly the same transition temperatures: $T_c^{A_5B}\sim 700$ K with the interaction set of Pt_8V, $T_c^{A_5B}\sim 650$ K with the interaction set of Pt_3V. To our knowledge, this ordered A_5B phase has never been reported in any system. An experiment using electron irradiation is in progress, in order to check the presence of this low-temperature phase.

Secondly, at $c=\frac{1}{3}$, the Pt_8V interaction set stabilizes the experimentally observed Pt_2Mo-type ordered phase. However, the calculated transition temperature is much lower than the experimental one: $T_c^{\rm cal}\sim 900$ K, i.e., 500 K below the experiment. With the Pt_3V interaction set, we find another ground state, labeled ''22'' in Kanamori's classification,[23] but which is nearly degenerate with the Pt_2Mo phase (the energy difference, per site, is smaller than 8 meV) and with a calculated transition temperature $T_c^{\rm cal}\sim 700$ K. In brief, our interaction sets lead to transition temperatures which are much lower than the experimental one. This discrepancy has already been observed in other systems: in Ni_2V (Ref. 24) and Ni_2Cr.[6] For unknown reasons, the presence at $c=\frac{1}{3}$ of the Pt_2Mo ordered phase leads systematically, within our inverse procedure, to abnormally low transition temperatures.

At $c=\frac{2}{5}$, we mention that a A_3B_2 composition (noted ''32'' in Ref. 23) is stabilized. That phase is stabilized with both sets of EPI's.

V. DISCUSSION

The ground-state analysis is summarized in Table III, together with the calculated and experimental transition temperatures. First, we note that both sets of interactions lead roughly to the same transition temperatures, except for the A_8B ordered state. This may be explained as follows.

We have a situation where the interactions are dominated by V_1 (see Fig. 6). In such a case, the number of AB first neighbors in a ground state is maximum for a given concentration c. More precisely, if the first-neighbor correlation function is defined by

$$x_1=\frac{1}{\mu_1 N}\sum_{mn}\sigma_m\sigma_n,$$

where the sum runs over all the first-neighbor pairs of a lattice of N sites and where $\mu_1=6$ is the first-neighbor degeneracy, x_1 takes a particular form for these ''well ordered'' states:

$$x_1^{\rm ord}=1-4c \quad \text{for } 0\leqslant c\leqslant\frac{1}{4},$$

whereas for the disordered state, we have

$$x_1^{\rm dis}=1-4c+4c^2 \quad (\forall c).$$

As a result, the influence of V_1 on the transition temperature decreases roughly with c^2. So, the transition temperatures of low concentration ordered phases, as the A_8B phase, is mainly governed by the interactions beyond V_1, i.e., by those interactions which are small in amplitude and, consequently, whose *relative* variations between our two interac-

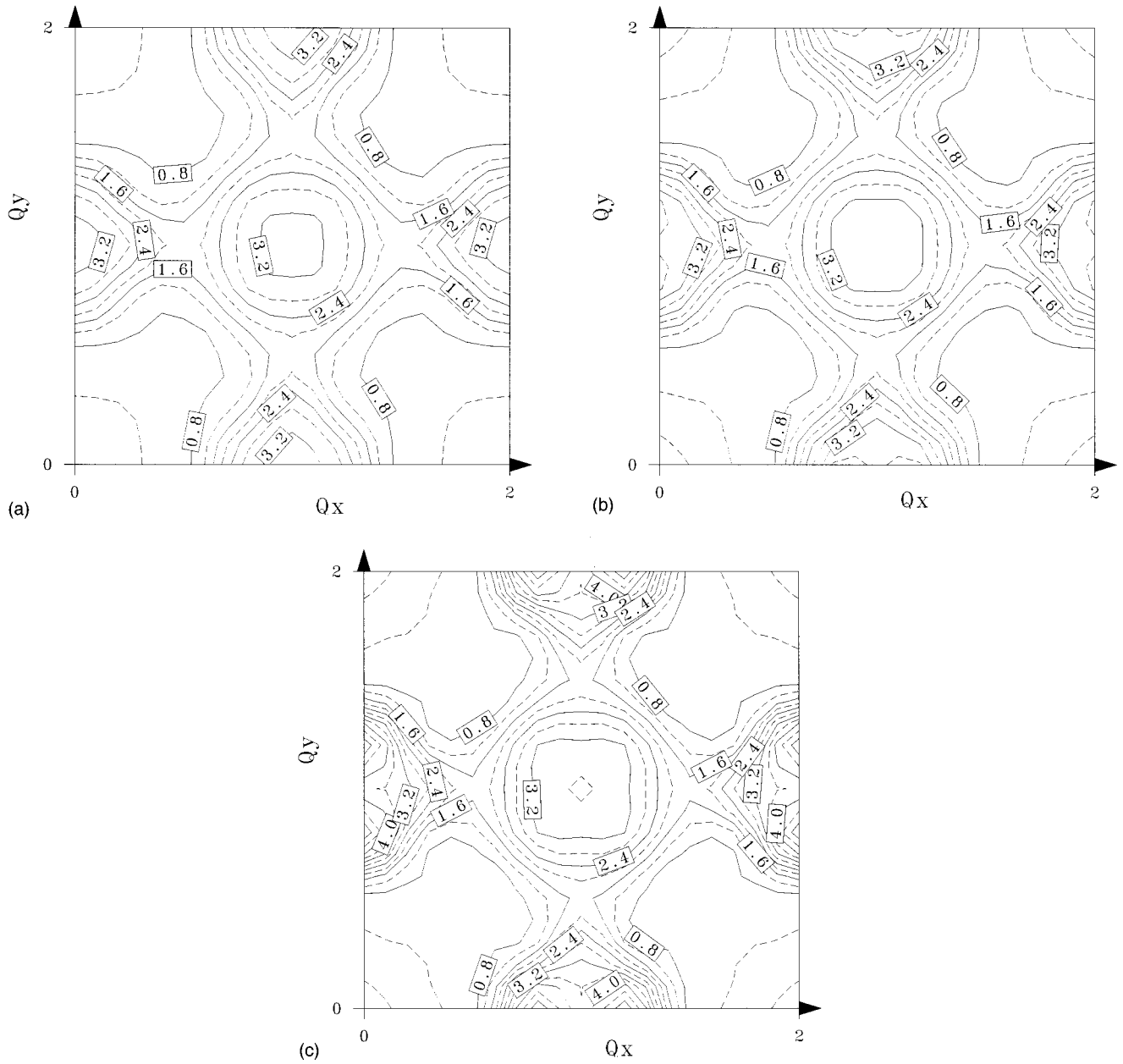

FIG. 7. Simulated SRO $\alpha(\vec{q})$ in the (100) plane, in Laue units, at the Pt_8V concentration, with the Pt_3V interaction set at (a) $T-T_c=250$ K, (b) $T-T_c=150$ K, (c) $T-T_c=50$ K.

tions sets are non-negligible. This is the reason why the calculated T_c of the A_8B ordered phase varies significantly between our two interactions sets.

As discussed above, the SRO intensity maxima in Pt_8V are located at incommensurate q points. As a result, these maxima are not locked by symmetries: they must shift when the temperature varies, as observed in our MC simulations (see Fig. 7).

We now discuss the origin and behavior of these incommensurate diffuse maxima. Within the Krivoglaz-Clapp and Moss (KCM) approximation, the SRO intensity $\alpha(\vec{q})$ is directly related to the Fourier transform

$$V(\vec{q})=\sum_{\vec{R}} V(\vec{R})e^{i\vec{q}\cdot\vec{R}}$$

of the pair interactions by

$$\alpha(\vec{q})=\frac{1}{1+4\beta c(1-c)V(\vec{q})}. \tag{4}$$

The diffuse intensity maxima coincide then with the minima of $V(\vec{q})$ and they are temperature and concentration independent. Obviously, we need to go beyond the KCM approximation in order to explain the present behavior of the intensity maxima. The cluster variation method (CVM) is, of course, a good candidate. Indeed, as shown below (see Fig. 8), a CVM analysis of $\alpha(\vec{q})$ with the Pt_3V interaction set, reproduces the split maxima observed in Pt_8V.

However, the CVM is a closed-form approximation and does not allow for a simple and direct analysis of the link

TABLE III. Ground states and calculated transition temperatures for different concentrations with the two sets found in Pt_8V and in Pt_3V. Comparison with experiment.

Concentration	1/9	1/6	1/4	1/3
Ground state and T_c with the Pt_8V interaction set	A_8B $T_c^{cal}\sim 850$ K	A_5B (13) $T_c^{cal}\sim 700$ K	$L1_2$ $T_c^{cal}\sim 1100$ K	PT_2Mo $T_c^{cal}\sim 900$ K
Ground state and T_c with the Pt_3V interaction set	A_8B $T_c^{cal}\sim 350$ K	A_5B (13) $T_c^{cal}\sim 650$ K	DO_{23} $T_c^{cal}\sim 1100$ K	22 $T_c^{cal}\sim 700$ K
Experimental ground state and T_c^{exp}	A_8B $T_c^{exp}=1090$ K		DO_{22} $T_c^{exp}=1288$ K	PT_2Mo $T_c^{exp}=1373$ K

between the V's and $\alpha(\vec{q})$. For that purpose, it is better to consider other approximations, which provide with an explicit relation between the V's and $\alpha(\vec{q})$. This is the case of the systematic expansion of $\alpha(\vec{q})^{-1}$ in power of β. Up to the second order in β, we have[25,26]

$$\alpha(\vec{q})^{-1}=1+4\beta c(1-c)V(\vec{q})-8\beta^2(1-2c)^2c(1-c)\times W_2(\vec{q})+16\beta^2c^2(1-c)^2\sum_{\vec{R}} V^2(\vec{R}), \tag{5}$$

where $W_2(\vec{q})$ is the Fourier transform of the squared pair interactions:

$$W_2(\vec{q})=\sum_{\vec{R}} V^2(\vec{R})e^{i\vec{q}\cdot\vec{R}}. \tag{6}$$

Equation (5) may be written in a more appealing form as follows:

$$\alpha(\vec{q})=\frac{1}{1+\Lambda+4\beta c(1-c)\tilde{V}(\vec{q})}, \tag{7}$$

where $\tilde{V}(\vec{q})$ is the Fourier transform of $\tilde{V}(\vec{R})$ defined by

$$\tilde{V}(\vec{R})=V(\vec{R})\{1-2(1-2c)^2\beta V(\vec{R})\} \tag{8}$$

and where Λ is a q-independent constant:

$$\Lambda=16\beta^2c^2(1-c)^2\sum_{\vec{R}} V^2(\vec{R}). \tag{9}$$

In other words, Eq. (7) looks like the KCM formula, except that $V(\vec{q})$, the Fourier transform of the actual pair interactions $V(\vec{R})$, has been replaced by $\tilde{V}(\vec{q})$, the Fourier transform of the ''renormalized'' pair interactions $\tilde{V}(\vec{R})$ given in Eq. (8). The key point now is that the stronger the interaction $V(\vec{R})$ is, the smaller the renormalization coefficient which affects $V(\vec{R})$ [see Eq. (8)] will be.

As a result, for a given concentration and temperature, the large interactions are more reduced than the small ones. In the present situation, we noted above that the first-neighbor interaction V_1 is dominant and positive. It means that at high temperature or high concentration, the properties of $\alpha(\vec{q})$ are mostly determined by V_1, while at low concentration or/and low temperature, the role of V_1 is much depressed: the maxima of $\alpha(\vec{q})$ will be more sensitive to the long-range interactions and will generally be incommensurate.

Before, to illustrate quantitatively the above discussion, we introduce a modification into Eq. (7), as in Ref. 27. The term Λ is no more defined by Eq. (9) but in such a way as to fulfill the sum rule on $\alpha(\vec{q})$:

$$\frac{1}{N}\sum_{\vec{q}} \alpha(\vec{q})=1. \tag{10}$$

However, this modification breaks the simple relation between the V's and $\alpha(\vec{q})$, since now Λ has to be determined by iterating Eqs. (7) and (10). In order to recover an explicit relation, we expand Eq. (10) to the second order in β and get

$$\Lambda\sim 16\beta^2c^2(1-c)^2\sum_{\vec{R}} \tilde{V}^2(\vec{R}). \tag{11}$$

This is very similar to the previous definition of Λ [see Eq. (9)], except that $V(\vec{R})$ is replaced by $\tilde{V}(\vec{R})$. Equations (7), (8), (11) define the high-temperature expansion (HTE) we use below.

We analyze now the diffuse intensity at $c=\frac{1}{9}$. Figure 8 shows $\alpha(\vec{q})$ along the line $(h00)$ in q space, calculated

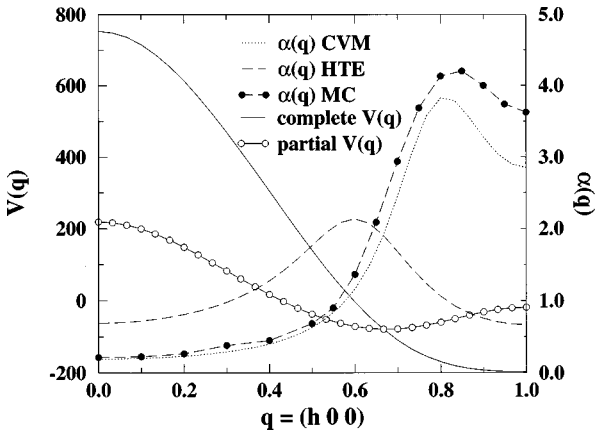

FIG. 8. Calculated $\alpha(\vec{q})$ along the $(h00)$ direction, within the CVM, the HTE and the MC simulations, at $c=\frac{1}{9}$ and 150 K above T_c, using the Pt_3V interaction set. Also displayed is the Fourier transform $V(\vec{q})$ of these interactions [noted ''complete $V(\vec{q})$''], along with a ''partial $V(\vec{q})$'' (same interactions, except V_1 which is set to zero).

within the previously defined HTE, with the Pt_3V interaction set and 150 K above the A_8B ordering temperature. The HTE reproduces qualitatively the split maxima, but the split amplitude is too large, as compared to the Monte Carlo and CVM results, which are almost equivalent (also displayed on Fig. 8). Yet, the fact that the HTE results display a splitting confirms the above analysis: the concentration and the temperature renormalize the V's in such a way that the role of V_1 is depressed. This is emphasized in Fig. 8, where we display the Fourier transform $V(\vec{q})$ along the $(h00)$ direction, with and without taking into account V_1. We note that the maximum of $\alpha(\vec{q})$ within the HTE method almost coincides with the minimum of $V(\vec{q})$ when V_1 is set to zero, whereas the minimum of the complete $V(\vec{q})$ is well located at $q=(100)$. As the temperature is raised, the influence of V_1 will increase and the maximum of $\alpha(\vec{q})$ will shift towards (100).

In brief, this analysis shows that a second-order HTE expansion of $\alpha(\vec{q})^{-1}$ is enough to explain the origin of the incommensurate split peaks of the diffuse intensity in Pt_8V.

Other systems, such as Cu_3Au,[28,29] Cu-Pd,[30] and Cu-Al,[32] display similar features. In particular, a recent experimental study of the split maxima of $\alpha(\vec{q})$ in Cu_3Au has recently been reported:[28] the main result was that the measured split distance, as referred to (100), increases when the temperature is raised, in contrast to the present situation. Theoretical studies on Cu_3Au and on Cu_3Pd,[31] as well as on Cu_3Al,[32,33] show also an increase of the split distance with increasing temperature. In those systems, the splitting occurs along the direction $(1k0)$ whereas, in Pt_8V, it occurs along the $(h00)$ axis. We argue now that, provided the first-neighbor interaction V_1 is dominant, this difference may be at the origin of the opposite behaviors of the split distance as a function of temperature.

The contribution to the Fourier transform $V(\vec{q})$ of the first-neighbor interaction V_1,

$$V_1(\vec{q})=V_1\sum_{1^{\text{st}}\text{neigh}} e^{i\vec{q}\cdot\vec{R}} \tag{12}$$

varies as a cosine along the $(h00)$ axis whereas it is constant along the $(1k0)$ direction:

$$V_1(h00)=4V_1[1+2\cos(\pi h)], \tag{13}$$

$$V_1(1k0)=-4V_1. \tag{14}$$

If $V_+(\vec{q})$, the Fourier transform of the interactions that extend beyond the first neighbors, is such that its minimum occurs for an incommensurate q point along the $(h00)$ axis, we have the above situation: if V_1 is large enough, the amplitude of the cosine term in Eq. (13) will be such that $V_+(\vec{q})$ plays no role for the determination of the minimum of the complete Fourier transform $V(\vec{q})$. At high temperature, $\alpha(\vec{q})$ will be maximum at (100). At low temperature, V_1 should be replaced by renormalized $\tilde{V}_1$: the amplitude of the cosine term is then reduced and the minimum of $\tilde{V}(\vec{q})$ will now be sensitive to $V_+(\vec{q})$ [more precisely to $\tilde{V}_+(\vec{q})$]. The maximum of $\alpha(\vec{q})$ will shift away from the (100) point. For any ordering system with a dominant first-neighbor interaction, a diffuse intensity maximum which at low enough temperature sits on an incommensurate q point *along the (h00) axis* should always shift towards (100) when the temperature is raised: the splitting distance, measured through (100), decreases with increasing temperature. In other words, the entropy erases the splitting, because, in that case, the splitting does not exist in the complete Fourier transform $V(\vec{q})$, but only in its component $V_+(\vec{q})$.

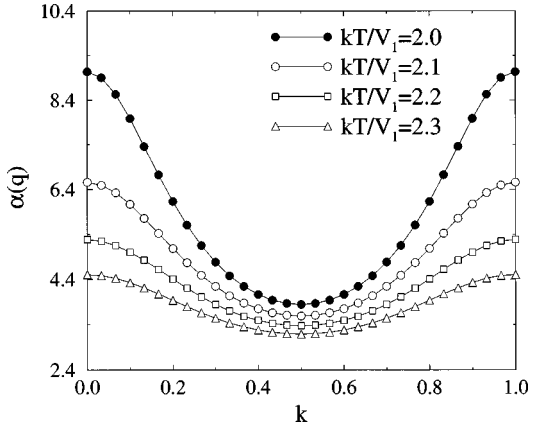

FIG. 9. CVM analysis of $\alpha(\vec{q})$ along the $(1k0)$ direction, with interaction between first neighbors V_1 only and for different temperatures (tetrahedron-octahedron approximation and $c=0.25$).

We consider now the other situation, where the diffuse intensity $\alpha(\vec{q})$ is maximum for an incommensurate q point that sits on the $(1k0)$ axis. This situation differs from the previous one in that $V_1(\vec{q})$ [see Eq. (14)] and, correspondingly, its counterpart $\tilde{V}_1(\vec{q})$ are constant along the $(1k0)$. Consequently, according to the KCM approximation and also to the second-order HTE, the fine features of $\alpha(\vec{q})$ along $(1k0)$ do not depend on V_1.

In particular, with first-neighbor interactions only, $\alpha(\vec{q})$ would be degenerated along $(1k0)$. We know that this is incorrect: within the CVM, this degeneracy is lifted and $\alpha(\vec{q})$ is maximum at (100).[34] A high-temperature expansion of $\alpha^{-1}(\vec{q})$ will recover this behavior only to order four in powers of β. An important point is that the amplitude of $\alpha(\vec{q})$ in the neighborhood of (100) is much more temperature dependent than, say, in the neighborhood of $(1\frac{1}{2}0)$. This is illustrated in Fig. 9, where we display $\alpha(\vec{q})$ along the $(1k0)$ axis, for different temperatures, as deduced from a CVM analysis with first-neighbor interactions only (within the tetrahedron-octahedron approximation).

Now, we may consider the role of weak interactions that extend beyond V_1, and such that their Fourier transform $V_+(\vec{q})$ is minimum for an incommensurate q point that sits on the $(1k0)$ axis. It is easy to understand that, due to the particular role of V_1 along the $(1k0)$ as shown in Fig. 9, the maximum of $\alpha(\vec{q})$ will be dictated by $V_+(\vec{q})$ only at high temperature, whereas, with decreasing temperature, the influence of V_1 will increase: the maximum of $\alpha(\vec{q})$ shifts towards (100). In brief, for any ordering system with dominant first-neighbor interactions, a diffuse intensity maximum that

sits, at high temperature, on an incommensurate q point *along the (1k0) axis* should always shift towards (100) with decreasing temperature: the splitting distance, measured through (100), increases with increasing temperature. In other words, the splitting is settled down by the entropy because, in that case, it pre-exists in the complete Fourier transform $V(\vec{q})$.

VI. CONCLUSION

We have measured the experimental SRO contributions in the Pt_3V and Pt_8V alloys. The Pt_3V SRO displays maxima at the (100) positions despite a ground state built with a $(1\frac{1}{2}\,0)$ concentration wave. The SRO features for Pt_8V are very different: the diffuse intensity displays split peaks around the (100) q point, with incommensurate maxima.

An important result of this work is that, despite two different SRO patterns, we have found that the EPI are almost concentration independent with a dominant and positive first-neighbor interaction V_1. The evolution of the diffuse intensity with composition is thus mainly due to the concentration and temperature sensitivity of the equilibrium state (i.e., the correlation functions). This unexpected concentration independence of the EPI has already been found in the Ni-Cr system.

Our results give us confidence in those interactions and more generally in our inverse methods: using a unique interaction set, we were able to (i) reproduce fine degeneracy effects between long period structures at the A_3B stoichiometry, (ii) stabilize the experimentally observed A_8B structure, (iii) reproduce the two different diffuse intensity maps at $c=\frac{1}{4}$ and $c=\frac{1}{9}$. Furthermore, these interactions stabilize a phase of composition A_5B, which has not been observed until now.

Moreover, we have analyzed the origin and behavior of the incommensurate maxima in Pt_8V within a high-temperature expansion up to the second order. We developed the diffuse intensity $\alpha(\vec{q})$ up to the second order in β, keeping the sum rule fulfilled to the same order. The resulting $\alpha(\vec{q})$ may be cast into a form equivalent to the well-known KCM formula, but with each actual pair interaction $V(\vec{R})$ replaced by a renormalized $\tilde{V}(\vec{R})$ proportional to $V(\vec{R})$, the coefficient of proportionality being temperature and concentration dependent. We show that the stronger $V(\vec{R})$ is, the smaller the coefficient of proportionality will be. In the case of Pt_8V, where V_1 is dominant and positive, the renormalized $\tilde{V}_1$ is much smaller than the original V_1. As a result, the influence of the other interactions increases significantly and the SRO maxima shift away from the (100) point to an incommensurate q point. Moreover, this HTE analysis shows that the splitting distance, measured through (100), decreases with increasing temperature, in agreement with our Monte Carlo simulations, and in contrast with other experimental and theoretical investigations in Cu_3Au, Cu-Pd, and Cu-Al.

More generally, we discuss these opposite temperature behaviors of the splitting distance in relation with the location in q space of the incommensurate maxima. Using simple arguments, and provided the first-neighbor interactions are dominant, we argue that the splitting distance [measured through (100)] increases with increasing temperature if the incommensurate maxima sit along the $(1k0)$ axis (as in Cu_3Au, Cu-Pd, and Cu-Al), whereas it decreases with increasing temperature if they sit along the $(h00)$ axis (or, more precisely, if they do not sit along the $(1k0)$ axis), as in Pt_8V.

ACKNOWLEDGMENTS

The authors are grateful to Francois Ducastelle and Igor Tsatskis for helpful discussions. We would like to thank D. Regen (ONERA Châtillon) for the growth of high-quality single crystals.

[1] D. Schryvers, and S. Amelinckx, Acta Metall. **34**, 43 (1986).
[2] J. Planés, A. Loiseau, F. Ducastelle, and G. Van Tendeloo, Inst. Phys. Conf. Ser. **90**, 261 (1987).
[3] E. Cabet and A. Loiseau, J. Phys. III **3**, C7-2051 (1993).
[4] E. Cabet, A. Pasturel, F. Ducastelle, and A. Loiseau, Phys. Rev. Lett. **76**, 3140 (1996).
[5] F. Solal, R. Caudron, F. Ducastelle, A. Finel, and A. Loiseau, Phys. Rev. Lett. **58**, 2245 (1987).
[6] R. Caudron, M. Sarfati, M. Barrachin, A. Finel, F. Ducastelle, and F. Solal, J. Phys. I **2**, 1145 (1992).
[7] A. Bieder and F. Gautier, Solid State Commun. **38**, 1219 (1981); Acta Metall. **35**, 1889 (1986).
[8] M. Barrachin, A. Finel, R. Caudron, A. Pasturel, and A. Francois, Phys. Rev. B **50**, 12 980 (1994).
[9] F. Ducastelle, *Order and Phase Stability in Alloys*, edited by F. R. de Boer and D. G. Pettifor, Cohesion and Structure **3** (North-Holland, Amsterdam, 1991).
[10] F. Ducastelle and F. Gautier, J. Phys. F **6**, 2039 (1976).
[11] J. C. Sparks and B. Borie, *Local Atomic Arrangements Studies by X-Ray Diffraction*, edited by J. B. Cohen and J. E. Hilliard (Gordon and Breach, London, 1966).
[12] L. H. Schwartz and J. B. Cohen, *Diffraction from Materials*, Materials Science Series (Academic, New York, 1977).
[13] W. Schweika and H. G Haubold, Phys. Rev. B **37**, 9240 (1988).
[14] B. Schönfeld, L. Reinhardt, and G. Kostorz, Phys. Status Solidi B **147**, 457 (1988).
[15] D. Le Bolloc'h, T. Cren, R. Caudron, and A. Finel, Comput. Mater. Sci. **8**, 24 (1997).
[16] S. C. Moss and P. C. Clapp, Phys. Rev. **171**, 764 (1968).
[17] V. I. Tokar, I. V. Masanskii, and T. A. Grishchenko, J. Phys. A **2**, 10 199 (1990).
[18] I. V. Masanskii, V. I. Tokar, and T. A. Grishchenko, Phys. Rev. B **44**, 4647 (1991).
[19] I. Tsatskis (unpublished).
[20] The energy differences (per site) between the DO_{22}, $L1_2$, and DO_{23} phases with a Hamiltonian up to the ninth-neighbor interactions are $\Delta(DO_{22}-DO_{23})=(-V_2+4V_3-4V_4-4V_6+8V_7$

$+2V_8)/2$, $\Delta(L1_2-DO_{22})=V_2-4V_3+4V_4+4V_6-8V_7$.
[21] N. M. Rosengaard and H. L. Skriver, Phys. Rev. B **50**, 4848 (1994); A. Pasturel (private communication).
[22] C. Wolverton, A. Zunger, and Z.-W Lu, Phys. Rev. B **49**, 16 058 (1994).
[23] J. Kanamori and Y. Kakehashi, J. Phys. A **38**, C7-274 (1977).
[24] M. Barrachin, Ph.D. thesis, Paris XI-Orsay, University, 1993.
[25] R. A. Tahir-Kheli, Phys. Rev. B **188**, 1142 (1969).
[26] M. Ferer and M. Wortis, Phys. Rev. B **6**, 3426 (1972).
[27] R. V. Chepulskii and V. N. Bugaev (unpublished).
[28] H. Reichert, S. C. Moss, and K. S. Liang, Phys. Rev. Lett. **77**, 4382 (1996).
[29] H. Reichert, I. Tsatskis, and S. C. Moss, Comput. Mater. Sci. **8**, 46 (1997).
[30] J. Kulik, D. Gratias, and D. De Fontaine, Phys. Rev. B **40**, 8607 (1989).
[31] V. Ozoliņš, C. Wolwerton, and A. Zunger, Phys. Rev. Lett. **79**, 955 (1997).
[32] H. Roelofs *et al.*, Scr. Metall. Mater. **34**, 1393 (1996); B. Schönfeld *et al.*, Acta Mater. **44**, 335 (1996).
[33] I. Tsatskis (unpublished).
[34] A. Finel and F. Ducastelle, Europhys. Lett. **1**, 135 (1986); **1**, 543(E) (1986); J. Phys. III **3**, C2-65 (1996).